Driven granular gases with gravity

A. Baldassarri,[1] U. Marini Bettolo Marconi,[1] A. Puglisi,[2] and A. Vulpiani[2]
[1]*Dipartimento di Matematica e Fisica, Università di Camerino, Via Madonna delle Carceri, I-62032 Camerino, Italy and Istituto Nazionale di Fisica della Materia, Unità di Camerino, Via Madonna delle Carceri, I-62032 Camerino, Italy*
[2]*Dipartimento di Fisica, Università La Sapienza, Piazzale Aldo Moro 2, 00185 Roma, Italy and Istituto Nazionale di Fisica della Materia, Unità di Roma, Piazzale Aldo Moro 2, 00185 Roma, Italy*
(Received 2 August 2000; revised manuscript received 16 January 2001; published 8 June 2001)

We study fluidized granular gases in a stationary state determined by the balance between external driving and bulk dissipation. The two considered situations are inspired by recent experiments, where gravity plays a major role as a driving mechanism: in the first case, gravity acts only in one direction and the bottom wall is vibrated; in the second case, gravity acts in both directions and no vibrating walls are present. Simulations performed under the molecular chaos assumption show averaged profiles of density, velocity, and granular temperature that are in good agreement with the experiments. Moreover, we measure velocity distributions that show strong non-Gaussian behavior, as experiments pointed out, but also density correlations accounting for clustering, at odds with the experimental results. The hydrodynamics of the first model is discussed and an exact solution is found for the density and granular temperature as functions of the distance from the vibrating wall. The limitations of such a solution, in particular in a broad layer near the wall injecting energy, are discussed.

DOI: 10.1103/PhysRevE.64.011301 PACS number(s): 81.05.Rm, 05.20.Dd

I. INTRODUCTION

In general, granular materials [1], due to the presence of dissipative forces, are not equilibrium systems neither from a configurational point of view or from a dynamical point of view. A statistically stationary state can be produced by a competition between the dissipation due to the inelastic collisions among the particles and the energy injection due to an external source, which prevents the system from cooling and coming to rest.

Usually, granular gases are considered in the homogeneous cooling regime; less frequently, they are studied in a stationary regime where energy flows into the system from some external source (stochastic driving, vibrating plates, shear, etc.) and dissipates by means of inelastic collisions. A sufficient condition to prevent strong density instabilities (such as those found by Du *et al.* [2]) seems to be the presence of an even minimal, but spread out, temperature source [4].

Much evidence, by mean of computer simulations, has been found to suggest that different kinds of density instabilities, such as *clustering* [5] (density gradients growing on time scales faster than typical hydrodynamics scales) or *inelastic collapse* [6] (the local divergence of the collision rate so that an infinite number of collisions occurs in a finite time), may emerge in a cooling granular assembly, that is, a granular gas losing its starting kinetic energy because of dissipative collisions. It has also been shown that the velocity distribution of particles in the free cooling state with homogeneous density has overpopulated high-energy tails $\sim \exp(-Av)$ [7,8].

When granular gases are driven in some way to balance the loss of energy due to collisions, a stationary state may be observed. The first model of randomly driven granular gas was proposed in [2]. It showed pathologies in the density and granular temperature profiles but also a breakdown of the thermodynamic limit. Another randomly driven model was then proposed to offer a different insight into the kinetics of granular gases [4]. In this model, the driving mechanism is a stochastic energy source acting on every particle as a heat bath with a fixed temperature T_F and a fixed viscous damping with characteristic time τ. In the stationary ''collisional'' regime (characterized by a collision time much lower than τ), the gas showed a fractal distribution of density and a distribution of velocities with overpopulated (non-Gaussian) high-energy tails. The homogeneous solution of the corresponding Boltzmann-Enskog equation has been analytically studied [8] showing that $\sim \exp(-Av^{3/2})$ high-energy tails are expected.

The aim of this work is to study a class of models for driven granular gases where the efficiency of the energy injection is guaranteed by the presence of gravity, taking inspiration from some recent experiments [9,10]: in these experiments, a bottom confining wall is the source of granular temperature while gravity forces the particles to return in contact with this source. We are interested in very diluted systems, where the granular material behaves as an inelastic gas, rather than dense granular flows, where many static effects, such as clogging, arching, or bubbling, appear. Such systems have been studied in relation to compaction dynamics or slow dense chute flows [3]. The study is based on direct simulation Monte Carlo, but we also discuss (for one of the models) the hydrodynamic theory. The first version of the model (gravity in only one direction and a vibrating bottom wall) has been previously studied in the one-dimensional case, which is a vibrated column of grains under the force of gravity [11], and the transition or the coexistence of different phases (gas, partially fluidized, and condensed) was investigated. In two dimensions, experiments [12], simulations [13], and theories [14] have analyzed a vertical system of grains with gravity and a vibrating bottom wall (with different kinds of vibration) searching for a simple

scaling relation between such global variables as the global granular temperature T_G or the center-of-mass height $h_{\mathrm{c.m.}}$ as a function of the size of the system N, the typical velocity of the vibrating wall V, or the restitution coefficient r. In all these calculations, the authors did not pay too much attention to the hydrodynamic profiles of the system, always assuming a constant granular temperature (''isotherm atmosphere'') and a density profile exponentially decaying with the height, as in the case of a Boltzmann elastic gas under gravity. One of the results of this work, discussed in Sec. V, is that also in the dilute regime, which one can study by means of Monte Carlo methods, the use of these assumptions is not obvious, in particular when trying to solve the global balance between external energy injection and bulk dissipation due to inelastic collisions among particles. It must also be noted that the general validity of a hydrodynamic description is still the subject of debate in the case of granular gases far from the elastic limit (a review of hydrodynamic problems is found in [15]).

In Sec. II, we present the two versions of the model. In Sec. III and IV, we illustrate the results. In Sec. V, we discuss the hydrodynamics of the model in its first version, and finally we draw conclusions. For the sake of completeness and in order to make the paper self-contained, we included in Appendix A a brief description of the direct simulation Monte Carlo of the Boltzmann equation, and in Appendix B we include the expressions of the dimensionless coefficients appearing in the hydrodynamic equations of Sec. V.

II. THE MODELS

We introduce two bidimensional models both consisting of N identical smooth disks of diameter σ and mass $m=1$ subject to binary instantaneous inelastic collisions that conserve the total momentum

$$\mathbf{v}_1'+\mathbf{v}_2'=\mathbf{v}_1+\mathbf{v}_2 \tag{1}$$

and reduce the normal component of the relative velocity

$$(\mathbf{v}_1'-\mathbf{v}_2')\cdot\hat{\mathbf{n}}=-r[(\mathbf{v}_1-\mathbf{v}_2)\cdot\hat{\mathbf{n}}], \tag{2}$$

where r is the normal restitution coefficient ($r=1$ in the completely elastic case) and $\hat{\mathbf{n}}=(\mathbf{x}_1-\mathbf{x}_2)/\sigma$ is the unit vector along the line of centers $\mathbf{x}_1$ and $\mathbf{x}_2$ of the colliding disks at contact. With these rules satisfied, the postcollisional velocities are

$$\mathbf{v}_1'=\mathbf{v}_1-\frac{1+r}{2}[(\mathbf{v}_1-\mathbf{v}_2)\cdot\hat{\mathbf{n}}]\hat{\mathbf{n}},$$

$$\mathbf{v}_2'=\mathbf{v}_2+\frac{1+r}{2}[(\mathbf{v}_1-\mathbf{v}_2)\cdot\hat{\mathbf{n}}]\hat{\mathbf{n}}. \tag{3}$$

In addition, the particles experience the external gravitational field and the presence of confining walls. With respect to previous works [4], the energy necessary to prevent the cooling of the system due to the inelastic collisions is not provided by a heat bath: in the present paper the energy feeding mechanism is of two types according to the two numerical experiments we perform.

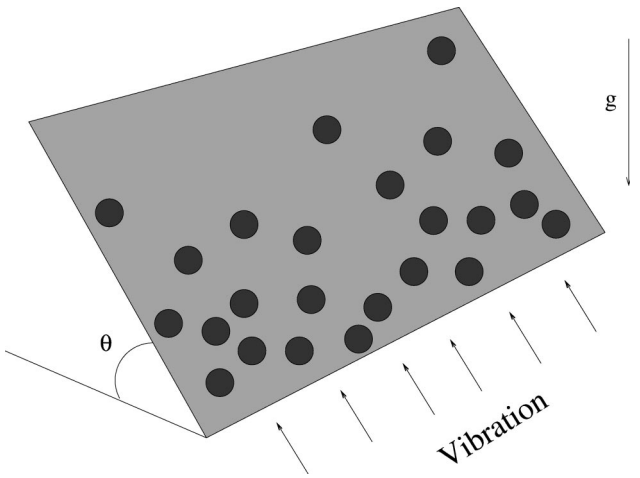

FIG. 1. A sketch of the first model where the granular assembly is driven by gravity plus a (periodically or stochastic) vibrating wall.

(i) In model A, illustrated in Fig. 1 and inspired by a recent laboratory experiment [9] and a numerical experiment [16], the ''apparatus'' consists of a plane of dimension $L_x \times L_y$ inclined by an angle θ with respect to the horizontal. The particles are constrained to move in such a plane under the action of an effective gravitational force $g_e=g\sin\theta$ pointing downward. In the horizontal direction, there are periodic boundary conditions. Vertically the particles are confined by walls, both inelastic with a restitution coefficient r_w (the difference between restitution coefficients for particle-particle interactions and particle-wall interactions will be discussed below). Besides, the bottom wall vibrates and therefore injects energy and momentum into the system. The vibration can have either a periodic character (as in [9]) or a stochastic behavior with thermal properties (as in [16]). In the periodic case, the wall oscillates vertically with the law $Y_w=A_w\sin(\omega_w t)$ and the particles collide with it as with a body of infinite mass, so that the vertical component of their velocity after the collision is $v_y'=-r_w v_y+(1+r_w)V_w$, where $V_w=A_w\omega_w\cos(\omega_w t)$ is the velocity of the vibrating wall. In the stochastic case, we assume that the vibration amplitude is negligible and that the particles colliding with the wall have, after the collision, new random velocity components $v_x\in(-\infty,+\infty)$ and $v_y\in(0,+\infty)$ with the following probability distributions:

$$P(v_y)=\frac{v_y}{T_w}\exp\left(-\frac{v_y^2}{2T_w}\right), \tag{4}$$

$$P(v_x)=\frac{1}{\sqrt{2\pi T_w}}\exp\left(-\frac{v_x^2}{2T_w}\right). \tag{5}$$

(ii) In model B, sketched in Fig. 2 the ''setup'' is a two-dimensional channel of depth L_y and of length L_x, vertically confined by a bottom and a top inelastic wall, with periodic

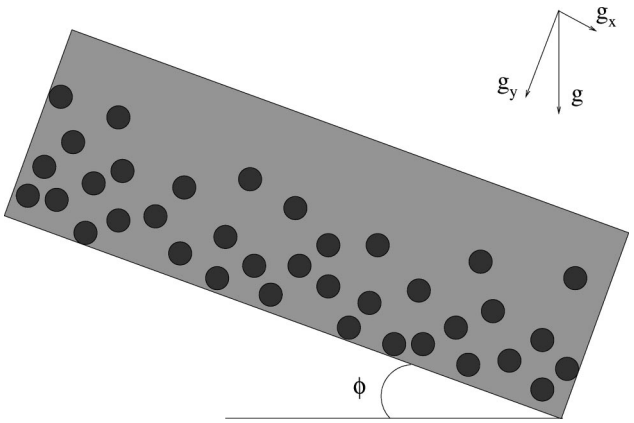

FIG. 2. A sketch of the second model where the only energy source is gravity, with components in both directions.

boundary conditions in the direction parallel to the flow. The channel is tilted up by an angle ϕ with respect to the horizontal so that gravity has both components $g_x = g \sin\phi$ and $g_y = g \cos\phi$. This model mimics the experiment performed by Azanza *et al.* [10], where a stationary flow in a two-dimensional inclined channel was observed at a point far from the source of the granular material. The assumption of periodic boundary conditions in the direction of the flow is consistent with the observed stationarity, due to the balance between the gravity drift and the damping effect of inelastic collisions (for a discussion of the possible regimes that can be shown by one particle in the presence of this balance, see [18]).

The chosen collision rule excludes the presence of tangential forces, and hence the rotational degrees of freedom do not contribute to the description of the dynamics.

Under the assumption of *molecular chaos*, stating that $P_2(\mathbf{x},\mathbf{x}+\sigma\hat{\mathbf{n}},\mathbf{v}_1,\mathbf{v}_2,t) = P(\mathbf{x},\mathbf{v}_1,t)P(\mathbf{x}+\sigma\hat{\mathbf{n}},\mathbf{v}_2,t)$, where P_2 and P are the probability density functions for two particles and one particle, respectively, it is possible to write down the Boltzmann equation [Eq. (9) in Sec. V], which can be solved by means of Monte Carlo methods. Here we used a simplified (but still efficient) version of the direct simulation Monte Carlo scheme proposed by Bird [17]. With respect to the original version of the algorithm, the clock that determines the collision rate is replaced by an *a priori* fixed collision rate via a constant collision probability p_c given to every disk at every time step Δt of the simulation, in such a way that the single-particle collision rate is $\chi \sim p_c/\Delta t$. The colliding particle then seeks its collision partner among the other particles in a neighborhood of radius r_B, choosing it randomly with a probability proportional to their relative velocities. Moreover, in this approximation the diameter σ is no longer explicitly relevant but it is directly related to the choices of p_c and r_B in a nontrivial way: in fact, the Bird algorithm allows the particles to pass through each other, so that a precise diameter cannot be defined and estimated as a function of p_c and r_B. The Bird scheme is described in more detail in Appendix A.

The agreement between our simulations and the inspiring experiments justifies the simplifying assumptions considered for our model, i.e., assuming molecular chaos and neglecting tangential forces. Nevertheless, as a partial check, we try a modified version of model B where the tangential forces may affect the postcollisional velocities of the particles. As reported below, the introduction of such forces does not change the behavior of the measured quantities.

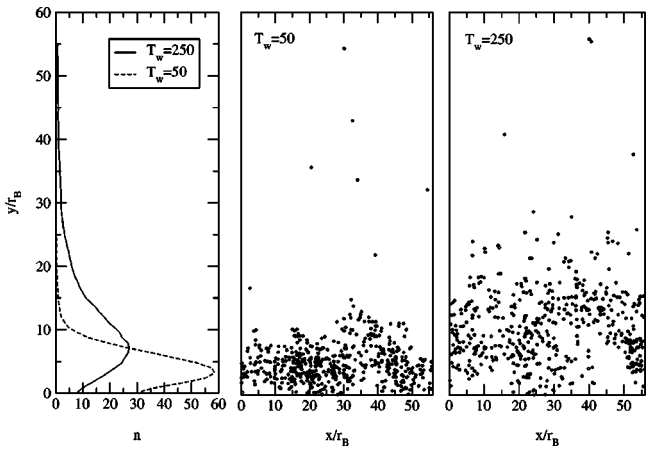

FIG. 3. Snapshots of the model A with stochastic wall at temperature $T_w = 50$ and $T_w = 250$. The leftmost inset displays the time-averaged number density profile for both cases. Values of other parameters are $N = 500$, $N_w \approx 56$, $r = 0.7$, $r_w = 0.7$, and $g_e = -1$.

III. DISCUSSION OF THE RESULTS: MODEL A

Simulations of the first model, an inclined plane with a bottom wall injecting energy, have been performed for different choices of the number of disks N, the normal restitution coefficient r, the dimensionless width of the plane $N_w = L_x/r_B$, and the parameter measuring the rate of energy injection from the wall, that is, the temperature T_w in the stochastic case and the amplitude and frequency A_w, ω_w in the periodic case.

Let us show how numerical simulations with the molecular chaos assumption reproduce the main results obtained in experiments [9,10] and in high-performance computer simulations [16] of inelastic hard disks.

Snapshots of the systems and time-averaged density profiles are shown in Fig. 3 for the case of a randomly vibrated wall. We are in the presence of a highly fluidized phase of the type Isobe and Nakanishi [16] call granular turbulent: looking at the time evolution of the density distribution of the system and of the coarse-grained velocity field, one observes an intermittency-like behavior with rapid and strong fluctuations of the density in the form of sudden explosions followed by large clusters of particles traveling downward, coherently, under the action of gravity. Of course, more dense and ordered phases (that one can expect at lower values of energy injection) are not reproducible with the direct simulation Monte Carlo, as strong excluded volume effects appear and the assumption of negligible short-range correlations fails.

In Figs. 4 and 5, we display the horizontal velocity distributions for the stochastic case. In Fig. 4, distributions for different T_w are shown: the data collapse is obtained by rescaling the velocities by $\sqrt{T_w}$. Instead, in Fig. 5 we show the

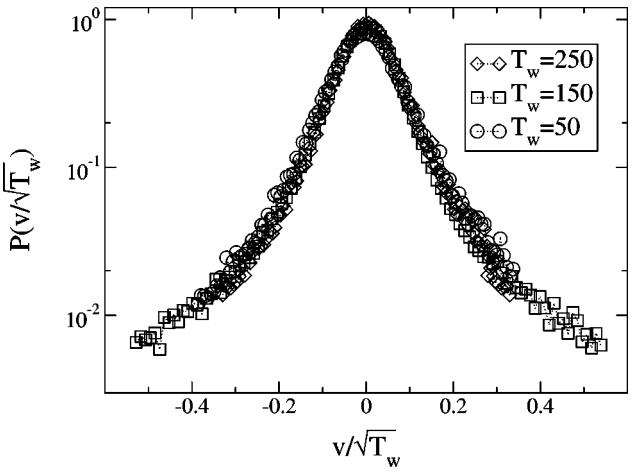

FIG. 4. Distribution of rescaled horizontal velocities $v/\sqrt{T_w}$ for the model A with stochastic wall at different temperatures $T_w=50$, $T_w=100$, and $T_w=250$. The other parameters are $N=5000$, $N_w\approx 180$, $r=0.7$, $r_w=0.7$, and $g_e=-1$.

velocity distributions of particles contained in stripes at different heights from the wall, again rescaled by $\sqrt{T(y)}$ (their own variance) in order to obtain the data collapse. It appears that the distributions are non-Gaussian and their broadening [that is the granular temperature $T(y)$] is density-dependent. This dependence is shown in Fig. 6 as well as its dependence upon the height. An analogous dependence has been shown in Ref. [4], where the granular gas was driven by a homogeneous heat bath, showing a power law $T\sim n^{-\beta}$ with $\beta\sim 0.8$, while in this case it seems $\beta\sim 0.88$.

The case of a periodically vibrated wall is illustrated in Figs. 7 and 8. One can see the density profiles (together with a snapshot of the system) and the distribution of horizontal velocities in two different regimes: for $g_e=-1$, a non-

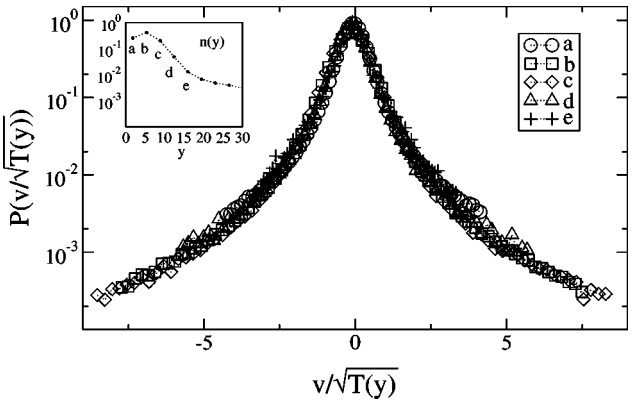

FIG. 5. Distribution of horizontal velocities, for the model A with stochastic wall, measured on stripes at different heights and rescaled by the average temperature at that height. The inset shows the normalized number density profile with the position of the chosen stripes. $N=5000$, $N_w\approx 180$, $r=0.7$, $r_w=0.7$, $g_e=-1$, and $T_w=100$.

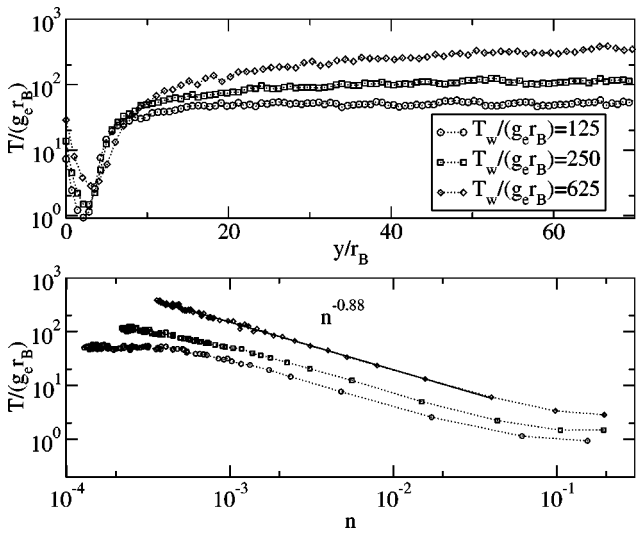

FIG. 6. Granular (dimensionless) temperature $T/(g_e r_B)$ versus dimensionless height y/r_B (above) and versus number density n (bottom) for the model A with stochastic wall, with $N=5000$, $N_w\approx 180$, $r=0.7$, $r_w=0.7$, and $g_e=-1$. The solid line is a power-law fit for $T(n)$.

Gaussian distribution is obtained, while a distribution close to a Gaussian appears when $g_e=-100$. This trend towards a Gaussian, as the angle of inclination is raised up, reproduces exactly the experimental observation of Kudrolli and Henry [9] (where the angle of inclination of the plane was raised up from $\theta=0.1°$ to $\theta=10°$) and can be explained as an effect of the increase of the collision rate with the wall, which ''randomizes'' the velocities in a more efficient way: this resembles the heath bath model [4], where one passes from the non-Gaussian regime to the Gaussian one increasing the ratio between the heating rate and the collision rate.

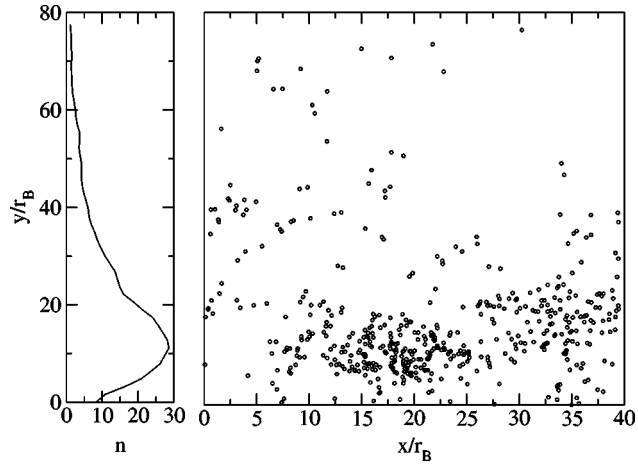

FIG. 7. Snapshot of the model A with periodically vibrating wall (right) and time-averaged density profile (left) for the following choice of parameters: $N=500$, $N_w\approx 56$, $r=0.5$, $r_w=0.7$, $g_e=-1$, $f_w=400\pi$, and $A_w=0.1$.

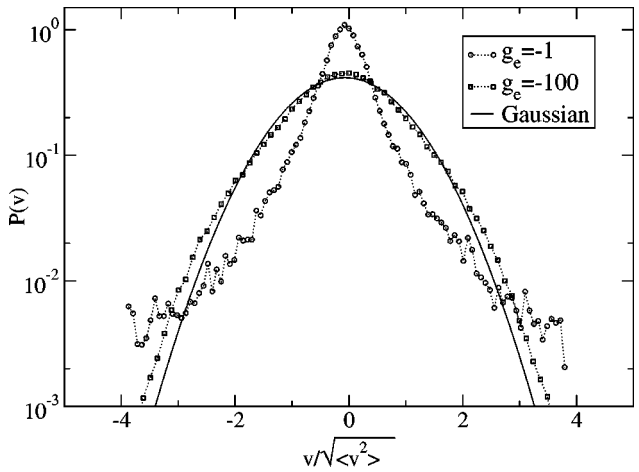

FIG. 8. Distributions of horizontal velocities for the model A with periodically vibrating wall for two different values of inclination, that is, $g_e=-1$ and $g_e=-100$, while the other parameters are fixed: $N=500$, $N_w\approx 56$, $r=0.5$, $r_w=0.7$, $f_w=400\pi$, and $A_w=0.1$.

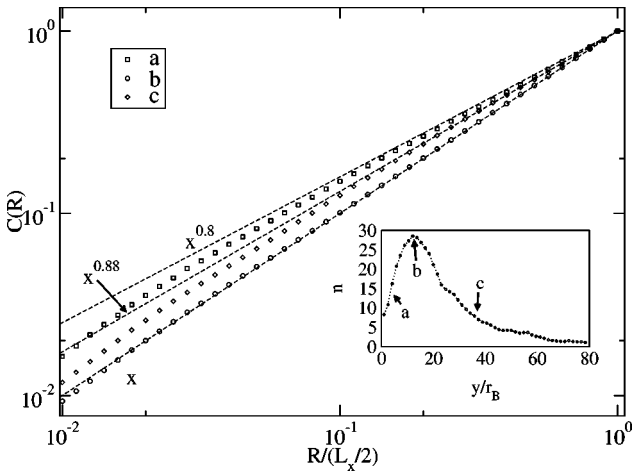

FIG. 9. Cumulated correlation function $C(R)$, as defined in the text, measured along stripes at different heights for the model A, with periodically vibrating wall. In the inset is displayed the number density profile, with the position of the chosen stripes. Here $N=500$, $N_w\approx 56$, $r=0.5$, $r_w=0.7$, $f_w=400\pi$, $A_w=0.1$, and $g_e=-1$.

In order to characterize the spatial clustering, we have studied the cumulated particle-particle correlation function,

$$C_{B(y,\Delta y)}(t,R)=\frac{1}{N_{B(y,\Delta y)}(N_{B(y,\Delta y)}-1)} \times \sum_{i\neq j:\mathbf{x}_i,\mathbf{x}_j\in B(y,\Delta y)} \Theta(R-|\mathbf{x}_i(t)-\mathbf{x}_j(t)|), \tag{6}$$

where $B(y,\Delta y)$ is a horizontal stripe contained between $y+\Delta y/2$ and $y-\Delta y/2$. After having checked that the system has reached a stationary regime, we have computed the time average of the correlation function, that is,

$$C_{B(y,\Delta y)}(R)=\frac{1}{T-t_0}\int_{t_0}^{T} dt\, C_{B(y,\Delta y)}(t,R), \tag{7}$$

which is independent of time if $T\gg t_0$. In Fig. 9, we show the $C(R)$ vs R for different stripes $B(y,\Delta y)$. We observe a power-law behavior

$$C_{B(y,\Delta y)}(R)\sim R^{d_2(y)}. \tag{8}$$

In the case of homogeneous density, d_2 is expected to be the topological dimension of the stripe, that is, $d_2=1$ if $R\gg\Delta y$ and $d_2=2$ if $R\ll\Delta y$.

Clustering, whose signature is a value of the correlation dimension d_2 lower than the topological dimension, appears in the stripes with not too high densities, where an exponent smaller than 1 is measured (the fit is performed in the region $R\gg\Delta y$). The evidence of clustering is at odds with the observation of Kudrolli and Henry [9]: They report, in fact, the absence of clustering by measuring the distribution of the number of particles in boxes of fixed dimensions spread all over the inclined plane. This observation is perhaps due to the fact that in the statistical analysis employed in Ref. [9], the number of particles in each box is considered disregarding their heights, that is, they may belong to regions of different densities. In such a way, the slow decaying tails, expected for the clusterized distributions of the stripes at lower densities, are partially hidden by the Poissonian (homogeneous) distribution of the stripes at higher density. Moreover, even from the global density distribution measured in their work, a tail decaying slower than a Poissonian cannot be clearly ruled out.

IV. DISCUSSION OF THE RESULTS: MODEL B

Let us now show the results for the second model, the inclined bidimensional channel.

In Figs. 10 and 11, the hydrodynamic fields $n(y)$ (number

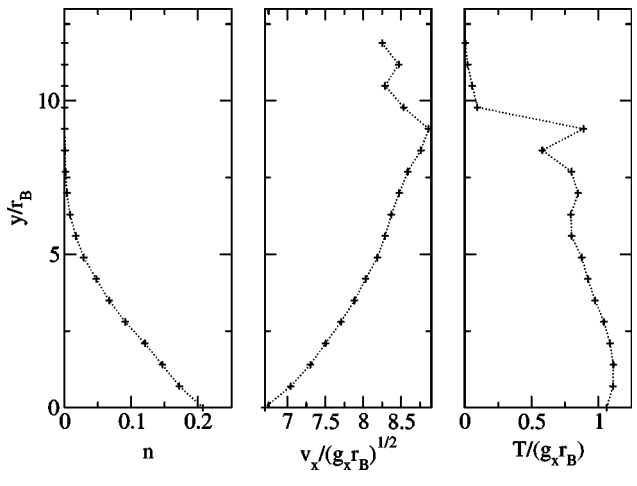

FIG. 10. Normalized number density n, dimensionless horizontal velocity $v_x/\sqrt{g_x r_B}$, and dimensionless granular temperature $T/\sqrt{g_x r_B}$ versus dimensionless height y/r_B for the two-dimensional inclined channel (model B): $N=500$, $N_w\approx 56$, $g_x=1$, $g_y=-2$ (i.e., the inclination angle $\phi=\pi/6$), $r=0.95$, and $r_w=0.95$.

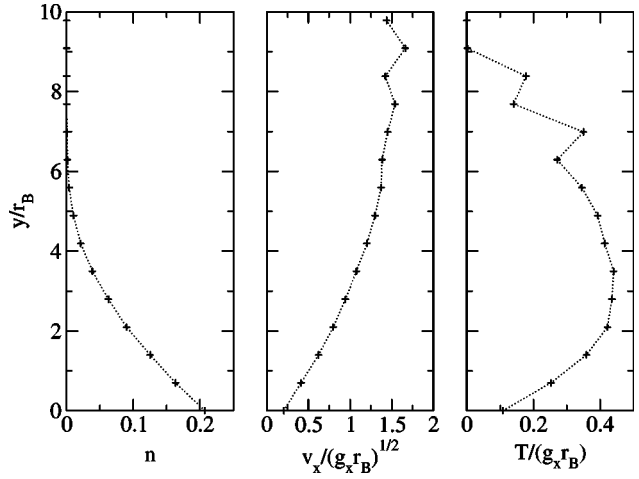

FIG. 11. Normalized number density n, dimensionless horizontal velocity $v_x/\sqrt{g_x r_B}$, and dimensionless granular temperature $T/\sqrt{g_x r_B}$ versus dimensionless height y/r_B for the two-dimensional inclined channel (model b): $N=500$, $N_w \approx 56$, $g_x=1$, $g_y=-2$ (i.e., the inclination angle $\phi=\pi/6$), $r=0.95$, and $r_w=0.4$.

density), $v_x(y)$ (velocity component parallel to the flow), and $T(y)$ (granular temperature) are shown as functions of the distance from the bottom wall y. The velocity, the temperature, and the height are made dimensionless by rescaling them by $\sqrt{g_x r_B}$, $g_x r_B$, and r_B, respectively. The profiles reproduce well those measured experimentally by Azanza *et al.* [10]: they show a critical height H of about six times the radius r_B, which corresponds to the separation between two different regimes of the cooling rate. In a mean-field framework, the local rate of dissipation due to the inelastic collisions (as already stated before) is $\zeta \propto nT^{3/2}$.

This can be understood by simply noting that the collision rate is proportional to the local density and to the local relative velocity of the particles ($\sqrt{T}$), while the change in the granular temperature induced by every collision is proportional to the temperature T. The quantity $\tilde{\zeta}=nT^{3/2}$ as a function of y is shown in Fig. 12. The cooling rate decreases exponentially and is reduced under 1/100 of its maximum value at about the observed critical height $H \approx 6 r_B$, accounting for the difference between a collisional regime and a ballistic one.

With respect to the velocity and temperature profiles in Fig. 10, we note here that quite unphysical features appear. In particular, the quite strong slipping effect near the bottom wall is in contrast with the experimental findings. We think that this is due to incorrect modeling of the particle-wall collision events.

The restitution coefficient used in our model has to be considered as an effective parameter describing the energetics of collisions. It should depend on the details of the collision event, in principle even on the relative velocities of the colliding particles. In the experiment, the bottom wall was covered with particles identical to the flowing ones with a spacing bounded between 0 and 0.8 mm. However, the particles are stuck to the bottom wall so that the collision event is completely different from a two-particle collision.

Using a lower effective restitution coefficient for the wall

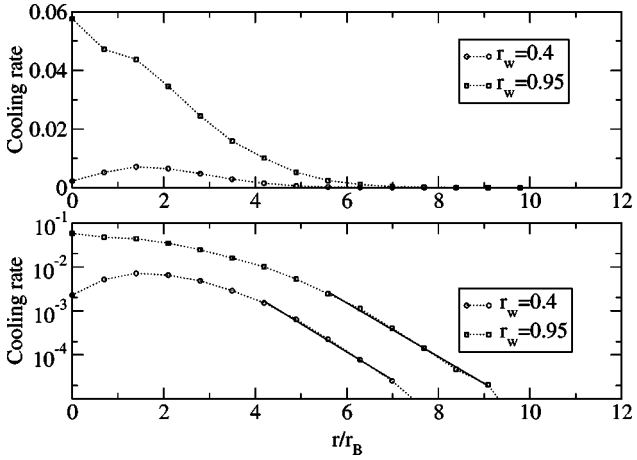

FIG. 12. Cooling rate, as defined in the text, versus dimensionless height y/r_B for the two-dimensional inclined channel (model B): $N=500$, $N_w \approx 56$, $g_x=1$, $g_y=-2$ (i.e., the inclination angle $\phi=\pi/6$), $r=0.95$, $r_w=0.95$, or $r_w=0.4$.

r_w (see Fig. 10), we obtain a better agreement with the experimental profiles. In particular, both temperature and velocity profiles seems to go to zero near the bottom, although we cannot really rule out slipping effects [$v_x(y=0) \neq 0$].

We have also studied the distribution of horizontal velocities in stripes at different heights (here the mean values are height-dependent). These are displayed in Fig. 13, showing the emergence of a non-Gaussian behavior mainly in the case with $r_w < r$ and only in the stripes near the bottom wall. The authors of the experiment of Ref. [10] claim that the distributions of velocity are very close to the Gaussian and try to fit their data with the rheological model proposed by Jenkins and Richman [19], which postulate a quasi-Gaussian equilibrium to calculate the transport coefficients. Near the bottom

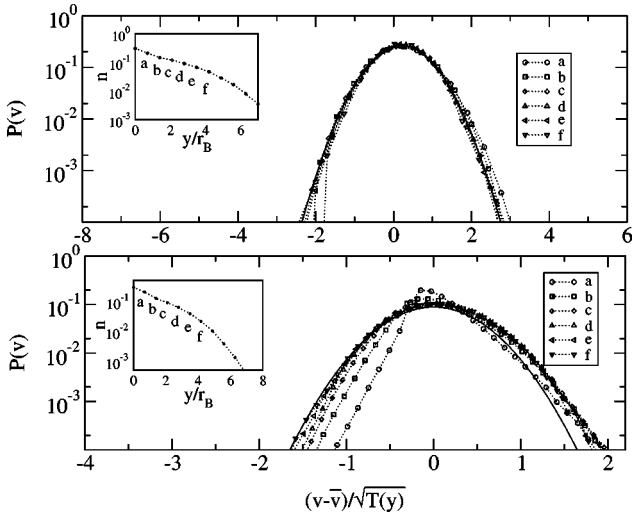

FIG. 13. Distribution of horizontal velocities for the model B, measured on stripes at different heights and rescaled in order to have the same mean and variance. The inset shows the normalized number density profile with the position of the chosen stripes. $N=500$, $N_w \approx 56$, $r=0.95$, $r_w=0.95$, $g_x=1$, and $g_y=-2$ (i.e., the inclination angle $\phi=\pi/6$).

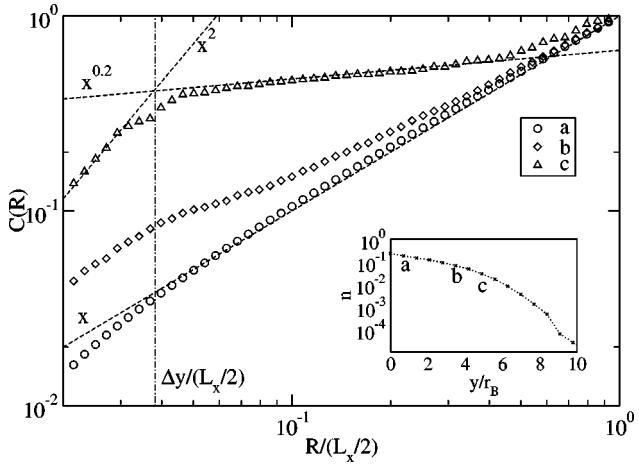

FIG. 14. Cumulated correlation function $C(R)$, as defined in the text, measured along stripes at different heights for the model B. In the inset is displayed the normalized number density profile with the position of the chosen stripes. Here $N=500$, $N_w \approx 56$, $r=0.95$, $r_w=0.95$, $g_x=1$, and $g_y=-2$ (i.e., the inclination angle $\phi=\pi/6$). The dashed lines represent the power-law fits, the vertical dot-dashed line represents the width of the stripes Δy.

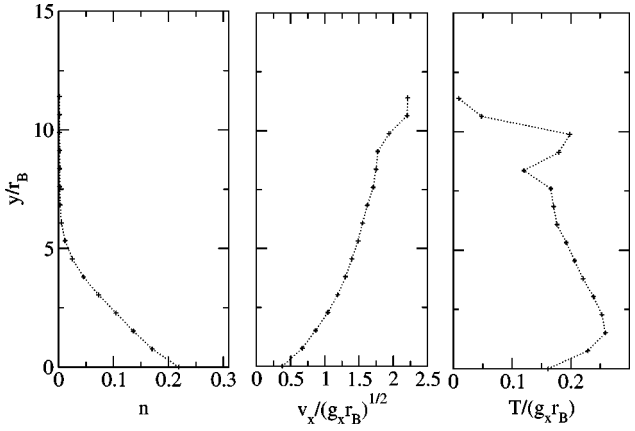

FIG. 15. Normalized number density n, dimensionless horizontal velocity $v_x/\sqrt{g_x r_B}$, and dimensionless granular temperature $T/(g_x r_B)$ versus dimensionless height y/r_B for the two-dimensional inclined channel. Here tangential restitution coefficients smaller than 1 are considered (see text): $N=500$, $N_w \approx 56$, $g_x=1$, $g_y=-2$ (i.e., the inclination angle $\phi=\pi/6$), $r^n=0.95$, $r^t=0$, $r_w^n=0.95$, and $r_w^t=0$.

wall, the Gaussian approximation is far from obvious, as shown by the results of our simulations: this is an effect of the inelasticity of the collisions but also of the proximity of the boundary.

Finally, we have investigated the homogeneity of the density: the Fig. 14 shows the previously defined function $C_{B(y,\Delta y)}(R)$ for stripes at different density. There appears again a clustering effect, with a correlation dimension ranging from 1 (homogeneous stripes) to 0.2 (highly clusterized stripes). In the figure, we show the very small distance region, $R<r_B$, where homogeneity should be recovered. Since in our simulation $\Delta y \approx r_B$, we expect $d(y)=2$ in this region.

We consider the comparison between our simplified model and the experimental profiles quite satisfactory: this seems to suggest that introducing further physical details should be irrelevant at this description level. However, we briefly report the results obtained with a slightly modified version of the model, including the effects of tangential forces. Such forces play a key role in dense granular flows [3,20], being responsible for arching. On the other hand, the present results suggest that in the case of diluted systems they act similarly to the normal forces without introducing noticeable effects.

The introduction of tangential forces in the model studied accounts for a new collision rule:

$$(\mathbf{v}_1'-\mathbf{v}_2')\cdot\hat{\mathbf{n}}=-r^n[(\mathbf{v}_1-\mathbf{v}_2)\cdot\hat{\mathbf{n}}],$$

$$(\mathbf{v}_1'-\mathbf{v}_2')\cdot\hat{\mathbf{t}}=-r^t[(\mathbf{v}_1-\mathbf{v}_2)\cdot\hat{\mathbf{t}}],$$

where we replace the single restitution coefficient with a pair of parameters r^n and r^t, respectively, due to the effect of normal and tangential collision forces ($\hat{t}$ is a unit vector perpendicular to $\hat{n}$). Analogously, the restitution coefficient r_w splits into two new parameters r_w^n and r_w^t. The results of simulations with several choices of the enlarged set of parameters do not show qualitative differences: setting tangential restitution coefficients lower than 1 is equivalent to enhancing the dissipation in the original model.

As an example of this, we show Fig. 15, where the extremal case of a vanishing tangential restitution coefficient is reported. Note that the profiles are similar to those shown in Fig. 11, where a low $r_w=0.4$ was used.

V. DISCUSSION OF THE HYDRODYNAMICS: RESULTS AND PROBLEMS

The Boltzmann equation for the two models introduced in this paper (in two dimensions) reads

$$\left(\frac{\partial}{\partial t}+\mathbf{v}\cdot\boldsymbol{\nabla}+g_i\frac{\partial}{\partial v_i}\right)f(\mathbf{x},\mathbf{v},t)=J(f,f), \tag{9}$$

$$J(f,f)=\sigma\int d\mathbf{v}_1\int d\hat{\mathbf{n}}\,\Theta(\hat{\mathbf{n}}\cdot\mathbf{v}_r)(\hat{\mathbf{n}}\cdot\mathbf{v}_r)$$
$$\times[r^{-2}f(\mathbf{x},\mathbf{v}',t)f(\mathbf{x},\mathbf{v}_1',t)-f(\mathbf{x},\mathbf{v},t)f(\mathbf{x},\mathbf{v}_1,t)]. \tag{10}$$

Here $\hat{\mathbf{n}}$ is the unit vector along the line joining the centers of the colliding particles at contact, $\mathbf{v}_r=\mathbf{v}-\mathbf{v}_1$ is the relative velocity of the colliding disks, Θ is the Heaviside step function, and $\mathbf{v}'$ and $\mathbf{v}_1'$ are the precollisional velocities leading after collision to velocities $\mathbf{v}$, $\mathbf{v}_1$.

Equation (9) must be completed with the boundary conditions in order to describe the microscopic evolution of the whole system.

The difficulty of solving the Boltzmann equation (9) can be bypassed by substituting the microscopic description given by $f(\mathbf{x},\mathbf{v},t)$ with the averaged macroscopic description given by the following hydrodynamic fields: the number

density field $n(\mathbf{x},t)$, the velocity field $\mathbf{v}(\mathbf{x},t)$, and the granular temperature field $T(\mathbf{x},t)$. These quantities are given by

$$n(\mathbf{x},t)=\int d\mathbf{v}\, f(\mathbf{x},\mathbf{v},t), \tag{11}$$

$$\mathbf{u}(\mathbf{x},t)=\frac{1}{n(\mathbf{x},t)}\int d\mathbf{v}\,\mathbf{v} f(\mathbf{x},\mathbf{v},t), \tag{12}$$

$$k_B T(\mathbf{x},t)=\frac{1}{n(\mathbf{x},t)}\int d\mathbf{v}\frac{m[\mathbf{v}-\mathbf{u}(\mathbf{x},t)]^2}{2} f(\mathbf{x},\mathbf{v},t). \tag{13}$$

Multiplying the Boltzmann equation (9) by 1 or $\mathbf{v}$ or $m[\mathbf{v}-\mathbf{u}(\mathbf{x},\mathbf{t})]^2/2$ and integrating over $\mathbf{v}_1$, one can derive [24,25] the equations of fluid dynamics:

$$\frac{Dn}{Dt}+n\partial_i u_i=0, \tag{14}$$

$$mn\frac{Du_i}{Dt}=-\partial_j\tau_{ij}+ng_i m \quad (i=1,2,3), \tag{15}$$

$$n\frac{Dk_BT}{Dt}=-\partial_i q_i-\tau_{ij}\partial_j u_i-\zeta n k_B T, \tag{16}$$

where $\partial_i=\partial/\partial x_i$ (for the sake of compactness, we use here the notation $x\to x_1$ and $y\to x_2$) and $D/Dt=\partial/\partial t+\mathbf{u}\cdot\boldsymbol{\nabla}$ is the Lagrangian derivative, e.g. $(D/Dt)F(\mathbf{x},t)=(d/dt)F(\phi(\mathbf{x}_0,t),t)$ with $\phi(\mathbf{x}_0,t)$ the evolution after a time t of $\mathbf{x}_0$ under the velocity field $\mathbf{u}$. In the above equations,

$$\tau_{ik}=\int d\mathbf{v}\, m(v_i-u_i)(v_k-u_k) f(\mathbf{x},\mathbf{v},t) \tag{17}$$

is the stress tensor, $\mathbf{g}$ is the volume external force (gravity in our case),

$$q_i=\int d\mathbf{v}\frac{m}{2}v_i|\mathbf{v}-\mathbf{u}|^2 f(\mathbf{x},\mathbf{v},t) \tag{18}$$

is the heat flux vector, and

$$\zeta(\mathbf{x},t)=\frac{m(1-r^2)\pi^{1/2}\sigma}{8\Gamma(5/2)nk_BT}\int d\mathbf{v}_1\int d\mathbf{v}_2|\mathbf{v}_1-\mathbf{v}_2|^3 \times f(\mathbf{x},\mathbf{v}_1,t)f(\mathbf{x},\mathbf{v}_2,t) \tag{19}$$

is the cooling rate due to dissipative collisions.

The set of equations (14)–(16) becomes closed hydrodynamic equations for the fields n, $\mathbf{u}$, and T when P_{ij}, $\mathbf{q}$, and ζ are expressed as functionals of these fields. This is obtained, for example, expressing the space and time dependence of f in terms of the hydrodynamic fields and then expanding f to first order (the so-called Navier-Stokes order) in their gradients, with the exception of ζ, which requires an expression of f to the second order of gradients to be consistent with the other terms. With this approximation, Eqs. (14)–(16) include the contributions up to the second order in the gradients of the fields.

Calculations of the closure of the hydrodynamic equations for granular media have been performed with some approximations restricting the validity of the results to the low dissipation or quasielastic limit [19]. More recently [21], the analysis has been extended to arbitrary inelasticity giving closed expressions for the momentum and heat fluxes and for the cooling rate ζ.

We follow these more recent results [21] and write down the hydrodynamics for the model A presented in this paper [gravity in one direction and vibrating bottom wall, i.e., $\mathbf{g}=(0,g_e)$ and $g_e<0$] with the following assumptions: the fields do not depend upon x (the coordinate parallel to the bottom wall), i.e., $\partial/\partial x=0$, and the system is in a steady state, i.e., $\partial/\partial t=0$. The continuity equation (14) then reads $\partial/\partial y(n(y)u_y(y))=0$ and this can be compatible with the bottom and top walls (where $nv_y=0$) only if $n(y)v_y(y)=0$, that is, in the absence of macroscopic vertical flow. The equations are written for the dimensionless fields $\tilde{T}=k_BT/(-g_e m\sigma)$ and $\tilde{n}=n\sigma^2$, while the position y is made dimensionless using $\tilde{y}=y/\sigma$. Finally, for the pressure we set $p(y)=\tau_{22}=n(y)k_BT(y)$. With the assumption discussed above, the equations of Brey *et al.* [21] read

$$\frac{d}{d\tilde{y}}[\tilde{n}(\tilde{y})\tilde{T}(\tilde{y})]=-\tilde{n}(\tilde{y}), \tag{20}$$

$$\frac{1}{\tilde{n}(\tilde{y})}\frac{d}{d\tilde{y}}Q_r(\tilde{y})+C(r)\tilde{n}(\tilde{y})\tilde{T}(\tilde{y})^{3/2}=0, \tag{21}$$

where $Q_r(\tilde{y})$ is the granular heat flux expressed by

$$Q_r(\tilde{y})=A(r)\tilde{T}(\tilde{y})^{1/2}\frac{d}{d\tilde{y}}\tilde{T}(\tilde{y})+B(r)\frac{\tilde{T}(\tilde{y})^{3/2}}{\tilde{n}(\tilde{y})}\frac{d}{d\tilde{y}}\tilde{n}(\tilde{y}). \tag{22}$$

In the above equations, $A(r)$, $B(r)$, and $C(r)$ are dimensionless monotone coefficients, all with the same sign, explicitly given in Appendix B. In particular, $B(1)=0$ and $C(1)=0$, i.e., in the elastic limit there is no dissipation and the heat transport is due only to the temperature gradients, while when $r<1$, a term dependent upon $(d/d\tilde{y})\ln(\tilde{n}(\tilde{y}))$ appears in $Q_r(\tilde{y})$. The use of dimensionless fields eliminates the explicit $\mathbf{g}$ dependence from the equations, which remains hidden in their structure [the right-hand term of Eq. (20), which is due to the gravitational pressure gradient, disappears in the equation for $g=0$].

A change of coordinate can be applied to Eqs. (20) and (21) in order to obtain a simpler form:

$$\tilde{y}\to l(\tilde{y})=\int_0^{\tilde{y}}\tilde{n}(y')dy'. \tag{23}$$

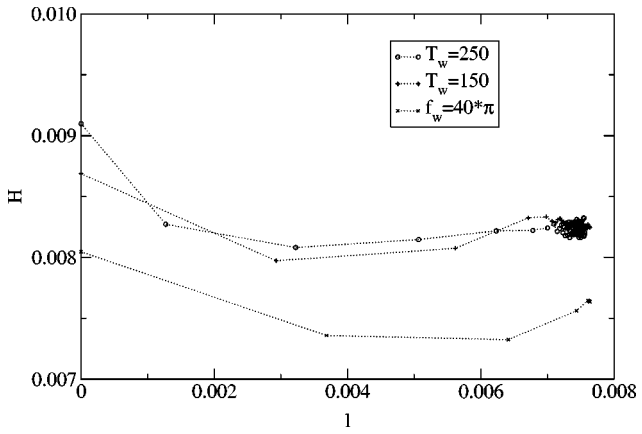

FIG. 16. Plot of H, defined in Sec. V, versus l, for three different simulations of the model A: two cases are with the stochastic wall ($N=5000$, $N_w \approx 180$, $r=0.7$, $r_w=0.7$, $g_e=-1$, $T_w=150$, and $T_w=250$), while the third case is with the periodic wall ($N=5000$, $N_w \approx 180$, $r=0.7$, $r_w=0.7$, $g_e=-1$, $f_w=80\pi$, and $A_w=0.1$).

It follows that when y spans the range $[0,L_y]$, the coordinate l spans the range $[0,\sigma/L_x]$. With this change of coordinate it happens that

$$\frac{d}{d\tilde{y}} \rightarrow \tilde{n}(l)\frac{d}{dl} \tag{24}$$

and the first Eq. (20) reads

$$\frac{d}{dl}[\tilde{n}(l)\tilde{T}(l)] = -1, \tag{25}$$

from which we immediately to see that

$$H = \tilde{n}(l)\tilde{T}(l) + l \tag{26}$$

is a constant, i.e. $(d/dl)H=0$. This is equivalent to observeing that

$$P(y) - g\int_0^y n(y')dy' \tag{27}$$

is constant, which is merely the Bernoulli theorem for a fluid in the gravitational field with the density depending upon the height.

Relation (26) is verified by the model simulated in this work in the Fig. 16 for almost all the height of the container, apart from the boundary layer near the bottom driving wall.

Using the coordinate l introduced in Eq. (23) and the elimination of $\tilde{n}(l)$ using the recognized constant, that is,

$$\tilde{n}(l) = \frac{H-l}{\tilde{T}(l)}, \tag{28}$$

the second Eq. (21), after some simplifications, and after a second change of coordinate $l \rightarrow s(l) = H - l$, becomes

$$\frac{\alpha(r)s}{\tilde{T}(s)^{1/2}}\frac{d^2}{ds^2}\tilde{T}(s) - \frac{\alpha(r)s}{2\tilde{T}(s)^{3/2}}\left(\frac{d}{ds}\tilde{T}(s)\right)^2 - \frac{\beta(r)}{\tilde{T}(s)^{1/2}}\frac{d}{ds}\tilde{T}(s) + s\tilde{T}(s)^{1/2} = 0, \tag{29}$$

where $\alpha(r) = [A(r) - B(r)]/C(r)$ and $\beta(r) = [A(r) - \frac{1}{2}B(r)]/[C(r)]$ are numerically checked to be positive (see Appendix B) for values of r not too low (about $r > 0.3$) and are divergent in the limit $r \rightarrow 1$.

Equation (29) become a linear equation in $\tilde{T}(s)$ as soon as the change of variable $z(s) = \tilde{T}(s)^{1/2}$ is performed:

$$2\alpha(r)s\frac{d^2}{ds^2}z(s) - 2\beta(r)\frac{d}{ds}z(s) + sz(s) = 0, \tag{30}$$

giving the solution

$$z(s) = As^{\alpha'}J_{\alpha'(r)}(\beta'(r)s) + Bs^{\alpha'(r)}N_{\alpha'(r)}(\beta'(r)s), \tag{31}$$

where $J_{\alpha'}$ and $N_{\alpha'}$ are the Bessel functions of the first and second kind, respectively, $\alpha'(r) = [\alpha(r) + \beta(r)]/[2\alpha(r)]$ is real and positive, and $\beta'(r) = \{1/[2\alpha(r)]\}^{1/2}$ is real and is considered in its positive determination. Moreover, they present the elastic values $\alpha'(1)=1$ and $\beta'(r \rightarrow 1)=0$ (see appendix B), while A and B are constants that must be determined by assigning the boundary conditions.

Then we can derive the expressions for $\tilde{T}(l)$ and $\tilde{n}(l)$:

$$\tilde{T}(l) = (H-l)^{2\alpha'(r)}[AJ_{\alpha'(r)}(\beta'(r)(H-l)) + BN_{\alpha'(r)}(\beta'(r)(H-l))]^2, \tag{32}$$

$$\tilde{n}(l) = \frac{(H-l)^{1-2\alpha'(r)}}{[AJ_{\alpha'(r)}(\beta'(r)(H-l)) + BN_{\alpha'(r)}(\beta'(r)(H-l))]^2}. \tag{33}$$

To calculate the expressions of $\tilde{T}$ and $\tilde{n}$ as a function of the original coordinate $\tilde{y}$, one needs to solve the equation

$$\frac{d}{dl}\tilde{y}(l) = \frac{1}{\tilde{n}(l)} \tag{34}$$

putting in it the solution (33). However, one can obtain a comparison with the numerical simulations using the new coordinate l. The main problem, at this point, is a discussion of the boundary conditions needed to eliminate the constants H, A, and B.

One could impose that $n(l_{\max})=0$ at $l_{\max}=\sigma/L_x$. From this condition it immediately follows that $H=\sigma/L_x$. A second condition can be obtained imposing a vanishing derivative of the temperature at $l_{\max}$, that is,

$$\left(\frac{d}{dl}\tilde{T}(l)\right)_{l=\sigma/L_x} = 0. \tag{35}$$

The third condition is the most delicate: it must contain the rate of energy injection coming from the vibrating wall. This rate depends upon the parameter T_w (or A_w and ω_w) and upon the particles flux impinging on the wall $\Phi = n_+ L_x \overline{v_+}$, where n_+ is the number density of particle approaching the wall and $\overline{v_+}$, is their velocity averaged near the wall. The first may be simply estimated as $n_+ = n(0)/2$. Moreover, if the velocity of the macroscopic flow is zero, the average velocity of the impinging particles is due only to fluctuations of u, that is, $\overline{v_+} \approx \sqrt{k_B T(0)/m}$. In a collision with the wall, the average energy gain is given by

$$\overline{\Delta E_w} = \frac{m}{2}(\overline{|\mathbf{v}'|^2 - |\mathbf{v}|^2}) = \frac{m}{2}[\overline{(v_x')^2} + \overline{(v_y')^2} - \overline{(v_x)^2} - \overline{(v_y)^2}], \tag{36}$$

which is different for the stochastic or the periodic case, respectively:

$$\overline{\Delta E_{ws}} = \frac{3 k_B T_w}{2} - k_B T(0), \tag{37}$$

$$\overline{\Delta E_{wp}} = \frac{m(1+r_w)^2 A_w^2 \omega_w^2}{4} - \frac{(1-r_w^2) k_B T(0)}{2} \tag{38}$$

obtained straightforwardly from Eq. (36) assuming no correlations between the velocity of the wall and that of the approaching particles.

Then a nonclosed expression for the rate of energy injection coming from the wall reads

$$W_{ws} = \overline{\Delta E_{ws}} \Phi = \tfrac{3}{4} k_B T_w L_x n(0) \sqrt{\frac{k_B T(0)}{m}} - \frac{L_x n(0)[k_B T(0)]^{3/2}}{2\sqrt{m}}, \tag{39}$$

$$W_{wp} = \overline{\Delta E_{wp}} \Phi = \frac{m(1+r_w)^2 A_w^2 \omega^2}{8} L_x n(0) \sqrt{\frac{k_B T(0)}{m}} - \frac{(1-r_w^2)}{4} L_x n(0) \frac{[k_B T(0)]^{3/2}}{\sqrt{m}}. \tag{40}$$

The above expressions are useful to establish the third needed boundary conditions. In order to do that, they must be compared with the energy dissipation rate due to inelastic collisions. The local dissipation rate is given by $\zeta(y) k_B T(y) = C(r) \sigma n(y) [k_B T(y)]^{3/2}/\sqrt{m}$ (see Appendix B). The instantaneous balance between energy injection and dissipation in collisions then reads

$$W = \frac{1}{L_x L_y} \int_0^{L_x} dx \int_0^{L_y} dy \, \zeta k_B T(y) = \frac{(-\sigma g)^{3/2} m C(r)}{L_y} \int_0^{\sigma/L_x} dl \, \tilde{T}(l)^{3/2}, \tag{41}$$

where W is W_{ws} or W_{wp}.

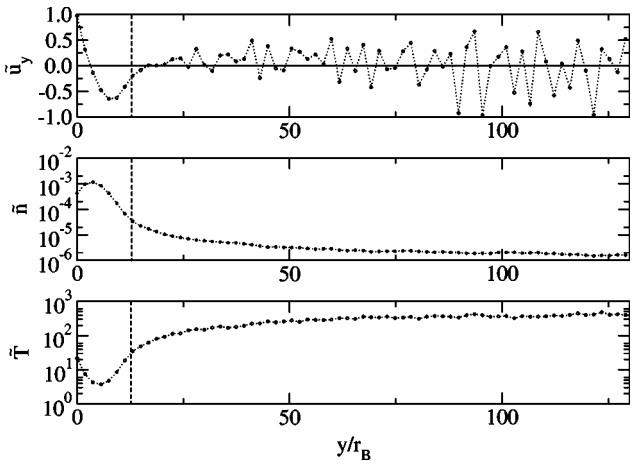

FIG. 17. Profiles of dimensionless hydrodynamic fields $\overline{n}$, $\overline{v_y}$, and $\overline{T}$ versus the dimensionless height y/r_B, for the model A with the stochastic wall at temperature $T_w = 250$. $N = 5000$, $N_w \approx 180$, $r = 0.7$, $r_w = 0.7$, and $g_e = -1$. The dashed vertical line marks the same height of Fig. 18.

Apart from the difficulty of solving the boundary conditions to give an expression of A and B as functions of the parameters of the model, one must observe that the hydrodynamic description given here is ill-posed from the beginning for what concerns a broad boundary layer near the bottom wall. A simple look at the profiles of $\overline{u_y}(\overline{y}) = u_y(\overline{y})/\sqrt{-g_e r_B}$ and $\overline{T}(\overline{y}) = T_y/(-g_e r_B)$ (the overlined quantities $\overline{n}$, $\overline{u}$, $\overline{T}$, and $\overline{y}$ are analogs of the dimensionless variables $\tilde{n}$, $\tilde{u}$, $\tilde{T}$, and $\tilde{y}$ with the assumption $m = 1$, $k_B = 1$, and $\sigma = r_B$) in Fig. 17 can give the idea. We expect from the continuity equation (14), as discussed above, $u_y(y) = 0$ for every y, while a broad region appears with a nonconstant and nonmonotonic behavior. Moreover, even the profile of $T(y)$ shows an extremal point, in this case a minimum. But from Eq. (22), taking into account the substitution (28), it can be seen that the imposition $(d/d\tilde{y})\tilde{T} = 0$ gives the following relation:

$$\tilde{T}(l)^{1/2} \frac{d^2}{dl^2} \tilde{T}(l) = \frac{C(r)}{B(r) - A(r)} \tilde{T}(l)^{3/2}, \tag{42}$$

where the fraction $C/(B-A) = -1/\alpha$ is numerically checked to be negative from a value of r lower than 0.4 (see appendix B). Relation (42) states that if $\tilde{T} > 0$, a minimum [that is, a positive value of $(d^2/dl^2)\tilde{T}$] cannot be expected. Similar profiles for $T(y)$, with a minimum, have been obtained in other simulations [22].

A tentative fit is presented in Fig. 18. Here we used three boundary conditions obtained directly from the simulations: a value of nT at a certain height y_1 to obtain directly H, the value of T, and the value of its derivative at heights y_2 and y_3, respectively, with all y_1, y_2, y_3 not far from the top wall. In this tentative fit, the problems discussed above appear clearly: there is a broad region near the bottom wall (see also

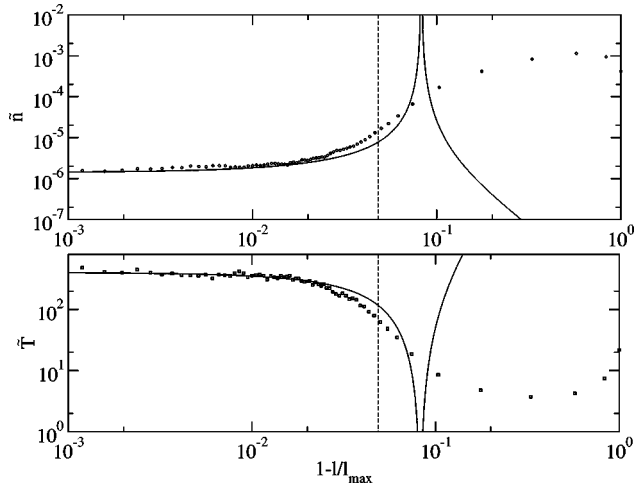

FIG. 18. Profiles of dimensionless hydrodynamic fields $\tilde{n}$ and $\tilde{T}$ versus $1-l/l_{\max}$ (the new coordinate l is defined in Sec. V and $l_{\max}=\sigma/L_x \approx r_B/L_x$) for the model A with the stochastic wall at temperature $T_w=250$. $N=5000$, $N_w \approx 180$, $r=0.7$, $r_w=0.7$, and $g_e=-1$. The solid lines are the theoretical fit using the hydrodynamics model of Brey *et al.* The vertical dashed line marks the height (also appearing in Fig. 17), where $\tilde{T}$ presents a minimum and, therefore, goes to 0.

Fig. 17) where the theoretical solution of Eqs. (20) and (21) is qualitatively different from the simulation data.

The qualitative inconsistencies between the observed profiles and the hydrodynamics in a broad boundary layer near the vibrating wall are probably due to the high-density gradients present in this region. The high-density gradients represent a numerical but also a conceptual problem: it is numerical because the profiles shown in Fig. 17 are obtained by means of a coarse graining in horizontal stripes $B(y,\Delta y)$ and so they can be compared to the theoretical profiles only if the density in these stripes is approximately homogeneous; it is conceptual because this hydrodynamic description is based upon the Navier-Stokes approximation, which is an expansion of $f(\mathbf{x},\mathbf{v},t)=f(\mathbf{v}|n(\mathbf{x},t),\mathbf{u}(\mathbf{x},t),T(\mathbf{x},t))$ up to the first order in the gradients of the fields $n,\mathbf{u},T$.

It must be stressed that this boundary-layer problem affects the description of the whole system in a strong way, as its global behavior (for example, the scaling laws for the global temperature or the center-of-mass height, extensively investigated in [11–14]) emerges from the balance between the bulk dissipation and the injection rate, which cannot be determined, even qualitatively, by a hydrodynamic study at the level proposed in this paper.

VI. CONCLUSIONS

We have studied, by means of a direct simulation Monte Carlo algorithm, a model of granular flow in two different bidimensional setups: the first version consists of an inclined plane with a periodic horizontal boundary condition, a top inelastic wall, and a vibrating bottom inelastic wall while gravity acts in the y direction perpendicular to the vibrating wall and pointing toward it; in the second version, gravity acts in both the x and y directions and the bottom wall does not vibrate, therefore resembling a stationary flow along a bidimensional channel. In both versions of the model, we have found good agreement with the analogous experiments [9,10]. In particular, the model with the vibrating wall shows strong non-Gaussian behavior of the velocities, which turns to a Gaussian behavior if the angle of inclination is raised up (this should be an effect of the increase of the heating rate, as the particles are more frequently in contact with the vibrating wall). The same model also presents evidence of different degrees of clusterization at different heights, and this is in contrast with the experimental observation [9]. The model with gravity in both directions and without a vibrating wall shows a stationary flow in the horizontal direction, where there are periodic boundary conditions: the profiles of the number density $n(y)$, the x component of the velocity $v_x(y)$, and the granular temperature $T(y)$ as functions of the distance from the bottom y are in very good agreement with the experimental profiles, showing a linear behavior in a broad region near the bottom that corresponds to the region where the collisions dominate the dynamics. This version of the model also shows strong evidence of density-dependent clusterization and a non-Gaussian behavior near the bottom wall. The simplicity of the first setup has allowed us to solve exactly the hydrodynamics equations for $n(y)$ and $T(y)$ following the formulation of Brey *et al.* [21]; however, it is not possible to obtain a matching condition between the bulk of the granular assembly and the vibrating wall that is responsible for the injection of energy. It seems to be an intrinsic problem of the high-density gradients observed near the bottom wall that the Navier-Stokes approximation fails to describe. This suggests the need for a better description of the boundary layer, which should include higher-order density and temperature gradients and also, at the level of kinetics, the non-Gaussian velocity statistics and the effect of spatial correlations (clustering).

ACKNOWLEDGMENTS

We wish to thank J. Brey, M. J. Ruiz Montero, and V. Loreto for useful discussions. This work was supported by the INFM through a PAIS grant.

APPENDIX A: BIRD'S SCHEME FOR THE MONTE CARLO SOLUTION OF THE BOLTZMANN EQUATION

Bird's scheme, often called direct simulation Monte Carlo (DSMC), was designed in the 1960s [17] and its derivation was *a priori* independent of the Boltzmann equation. Recently, its convergence to solutions of the Boltzmann equation in a suitable limit has been proved [23], reinterpreting it as a measure-valued stochastic process.

Bird's scheme can be formulated as a fixed time (Δt) step ''molecular-dynamics-like'' simulation. At each time step, the dynamics is separated into two distinct processes: the independent evolution of every particle and the collisions of near particles. The following algorithm (for the single time step) is the one we implemented in this work, which is a modification of the original scheme.

(i) Free flow Each particle evolves independently follow-

ing the equations of motion $\dot{\mathbf{x}}=\mathbf{v},\dot{\mathbf{v}}=\mathbf{g}$ with first-order discretization.

(ii) Collisions. Every particle i, during this time step, has a probability p_c of making a collision, so that $p_c/\Delta t \propto \sigma$ (in fact, the collision cross section is proportional to the diameter of the particles). If the particle collides, then another particle $\mathbf{x}_j,\mathbf{v}_j$ is chosen with $|\mathbf{x}_i-\mathbf{x}_j|\leqslant r_B$ (we call r_B the ''Bird radius,'' but it could also be thought of as the ''Boltzmann radius'') with probability $p_{ij}\propto|\mathbf{v}_r|$; for the pair i,j, the postcollisional velocities are calculated as they were at in contact with a random choice of the collision parameter $\hat{\mathbf{n}}$; this step is repeated for every particle.

It is important to stress the fact that this is above all a Monte Carlo method to solve the Boltzmann equation (9). In this sense, microscopic (short-range) details are lost; the N particles themselves do not represent N real grains of the granular assembly but carry the space-time average information of many more particles.

APPENDIX B: THE NUMERICAL COEFFICIENTS IN THE HYDRODYNAMIC EQUATIONS

In Sec. V, the hydrodynamics of the first model is studied. The equations with the transport coefficients calculated by Brey *et al.* [21] are used. The coefficients needed in our case are the two thermal conductivities κ and μ appearing in the expression of the heat flux,

$$\mathbf{q}=-\kappa\boldsymbol{\nabla}(k_BT)-\mu\boldsymbol{\nabla}n, \tag{B1}$$

and the coefficient ζ of the dissipative term,

$$-\zeta k_BT. \tag{B2}$$

In Ref. [21], the coefficients are given for the case $d=3$ (d is the dimension of the space). We have taken the coefficients for $d=2$ from an unpublished (to our knowledge) work of Brey *et al.* [26], and we have put them in the following form:

$$-\kappa=A(r)\frac{(k_BT)^{1/2}}{\sigma m^{1/2}}, \tag{B3}$$

$$-\mu=B(r)\frac{(k_BT)^{3/2}}{\sigma m^{1/2}n}, \tag{B4}$$

$$-\zeta=C(r)\frac{\sigma n(k_BT)^{1/2}}{m^{1/2}}, \tag{B5}$$

where

$$A(r)=-\kappa_1(r)\kappa_0, \tag{B6}$$

$$B(r)=-\mu_1(r)\kappa_0, \tag{B7}$$

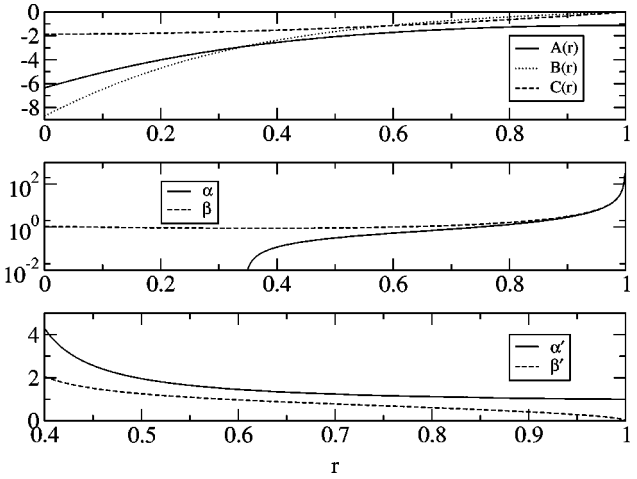

FIG. 19. Transport coefficients A, B, and dissipative coefficient C of hydrodynamics (Sec. V), numerical coefficients α and β of Eq. (30), and numerical coefficients α' and β' of the solution (31) versus the restitution coefficient r.

$$C(r)=-\zeta_1(r)/\eta_0, \tag{B8}$$

and

$$\kappa_0\frac{2}{\sqrt{\pi}}, \tag{B9}$$

$$\eta_0=\frac{1}{2\sqrt{\pi}}, \tag{B10}$$

$$\mu_1=2\frac{\zeta_1(r)\left(\kappa_1(r)+\dfrac{c_1(r)}{4\zeta_1(r)}\right)}{\nu_1(r)-3\zeta_1(r)}, \tag{B11}$$

$$\kappa_1=\frac{1+c_1(r)}{\nu_1(r)-4\zeta_1(r)}, \tag{B12}$$

$$\zeta_1=\tfrac{1}{2}(1-r^2)[1+\tfrac{3}{32}c_1(r)], \tag{B13}$$

$$\nu_1(r)=(1+r)[\tfrac{19}{8}-\tfrac{15}{8}r+\tfrac{1}{1024}(14-6r)c_1(r)], \tag{B14}$$

$$c_1(r)=32\frac{(1-r)(1-2r^2)}{57-25r+30r^2(1-r)}. \tag{B15}$$

The coefficients $A(r)$, $B(r)$, and $C(r)$ are plotted in Fig. 19. In the same figure are also presented the coefficients $\alpha(r)=[A(r)-B(r)]/C(r)$ and $\beta(r)=[A(r)-\frac{1}{2}B(r)]/C(r)$ appearing in Eq. (30) and, finally, the coefficients $\alpha'(r)=[\alpha(r)+\beta(r)]/[2\alpha(r)]$ and $\beta'(r)=\{1/[2\alpha(r)]\}^{1/2}$ appearing in the solution (31).

[1] for a general overview, see H.M. Jaeger, S.R. Nagel, and R.P. Behringer, Rev. Mod. Phys. **68**, 1259 (1996), and references therein.
[2] Y. Du, H. Li, and L.P. Kadanoff, Phys. Rev. Lett. **74**, 1268 (1995).
[3] T.G. Drake, J. Geophys. Res. B **95**, 8681 (1900); T. Pöschel, J. Phys. II **3**, 27 (1993).
[4] A. Puglisi, V. Loreto, U. Marini Bettolo Marconi, A. Petri, and A. Vulpiani, Phys. Rev. Lett. **81**, 3848 (1998); A. Puglisi, V. Loreto, U. Marini Bettolo Marconi, and A. Vulpiani, Phys. Rev. E **59**, 5582 (1999).
[5] I. Goldhirsch and G. Zanetti, Phys. Rev. Lett. **70**, 1619 (1993).
[6] S. McNamara and W.R. Young, Phys. Fluids A **4**, 496 (1992); **5**, 34 (1993); S. McNamara and W.R. Young, Phys. Rev. E **50**, R28 (1994).
[7] S.E. Esipov and T. Pöschel, J. Stat. Phys. **86**, 1385 (1997).
[8] T.P.C. van Noije and M.H. Ernst, Granular Matter **1**, 57 (1998).
[9] A. Kudrolli and J. Henry, Phys. Rev. E **62**, R1489 (2000).
[10] E. Azanza, F. Chevoir, and P. Moucheront, in *Powder & Grains 97*, edited by R. P. Behringer and J. T. Jenkins (Balkema, Rotterdam, 1997).
[11] S. Luding, E. Clément, A. Blumen, J. Rajchenbach, and J. Duran, Phys. Rev. E **49**, 1634 (1994); B. Bernu, F. Delyon, and R. Mazighi, *ibid.* **50**, 4551 (1994).
[12] S. Warr, J.M. Huntley, and G.T.H. Jacques, Phys. Rev. E **52**, 5583 (1995).
[13] S. McNamara and S. Luding, Phys. Rev. E **58**, 813 (1998).
[14] V. Kumaran, Phys. Rev. E **57**, 5660 (1998); P. Sunthar and V. Kumaran, *ibid.* **60**, 1951 (1999).
[15] I. Goldhirsch, Chaos **9**, 659 (1999).
[16] M. Isobe and H. Nakanishi, J. Phys. Soc. Jpn. **68**, 2882 (1999).
[17] G.A. Bird, Phys. Fluids **13**, 2676 (1970); C. Cercignani, R. Illner, and M. Pulvirenti, *The Mathematical Theory of Dilute Gases* (Springer-Verlag, New York, 1994).
[18] U. Marini Bettolo Marconi, M. Conti, and A. Vulpiani, Europhys. Lett. **51**, 685 (2000).
[19] J.T. Jenkins and S.B. Savage, J. Fluid Mech. **130**, 187 (1983); C.K.K. Lun, S.B. Savage, D.J. Jeffrey, and N. Chepurniy, *ibid.* **140**, 223 (1984); J.T. Jenkins and M.W. Richman, Phys. Fluids **28**, 3485 (1985); C.K.K. Lun and S.B. Savage, J. Appl. Mech. **154**, 47 (1987); J.T. Jenkins and M.W. Richman, J. Fluid Mech. **192**, 313 (1988).
[20] J. Schäfer, S. Dippel, and D.E. Wolf, J. Phys. I **6**, 5 (1996).
[21] J.J. Brey, J.W. Dufty, C.S. Kim, and A. Santos, Phys. Rev. E **58**, 4638 (1998).
[22] R. Soto, M. Mareschal, and D. Risso, Phys. Rev. E **83**, 5003 (1999).
[23] W. Wagner, J. Stat. Phys. **66**, 1011 (1992).
[24] S. Chapman and T. G. Cowling, *The Mathematical Theory of Non Uniform Gases* (Cambridge University Press, Cambridge, 1958).
[25] C. Cercignani, *The Boltzmann Equation and Its Applications* (Springer-Verlag, New York, 1988).
[26] J. J. Brey, M. J. Ruiz-Montero, and F. Moreno (unpublished).